CARDIOVASCULAR SIMULATION STUDY OF INFANTS WITH TRANSPOSITION OF THE GREAT ARTERIES AFTER SURGICAL CORRECTION†

E. H. BLACKSTONE*, A. K. GUPTA** and V. C. RIDEOUT**

After the Mustard operation in infants for transposition of the great arteries (TGA), unusually contoured pressure waveforms are observed. We studied this phenomenon by devising a pressure flow model of the infant circulation into which was incorporated a model of the Mustard operation. This latter model dealt in particular with pressure coupling across the initially flexible baffle material used to repartition to the atria and also with the changes in coupling which occur as the baffle material stiffens. The models were implemented on a hybrid computer system. A reasonable approximation to the unusual waveforms observed clinically was found during simulation experiments. The model has given us new insight into the physiological consequences of the Mustard operation and has yielded a reasonable hypothesis for explaining the clinical observations.

1. INTRODUCTION

Transposition of the great arteries (TGA) is one of the most common congenital heart defects, occuring in about 15% of newborns with cardiac malformations [1]. In this condition, venous inflows to the heart are normal but arterial outflows are reversed. By way of explanation, in the normal circulation oxygen depleted blood is pumped by the right ventricle through the pulmonary artery to the lungs. Oxygenated blood returns from the lungs to the heart and is pumped by the left ventricle through the aorta to the body. The entire system is one complete loop or a series circuit. In contrast, transposition of the two great arteries, pulmonary artery and aorta, results in two circulatory loops in parallel one through the lungs, the other through the body. Survival of such infants is dependent upon the presence of communication between the two sides of the heart. In about half the

This research was supported in part by Program Project Grant HL 11,310 National Institutes of Health and by the Engineering Experiment Station of the University of Wisconsin.

† Reprinted from SIMULATION OF SYSTEMS, edited by L. Dekker. 8th AICA Congress, Delft, August 23-28, 1976, organized by Computing Center Delft University of Technology, North Holland Publishing Company, Amsterdam, 1976.

* Department of Surgery, University of Alabama School and Medical Center, Birmingham, Alabama, U.S.A.

** Department of Electrical and Computer Engineering, University of Wisconsin, Madison, Wisconsin, U.S.A.

cases a ventricular septal defect is present. When the ventricular septum is intact a communication between the left and right atria is created by a ballon-catheter device as an emergency procedure shortly after birth [2].

Surgical correction of the defect is attempted at one year of age, on the average, by an operation which repartitions the atria in such a fashion that the venous returns from the body and the lungs are transposed. This operation, called the Mustard operation, puts the two parallel loops into a single series circuit [3, 4]. (An operations simply to switch the aorta and pulmonary arteries is not clinical feasible in most cases [5]).

The atrial repartitioning is accomplished with a piece of either dacron cloth or pericardium. These materials are initially quite flexible and as sewn in take the form of a complex three-dimensional baffle. This baffle moves to and fro during the various phases of the cardiac cycle early post-operatively. Figure 1 shows the electrocardiogram and pressure waveforms in an infant immediately after the Mustard operation [6]. Notice in partic-

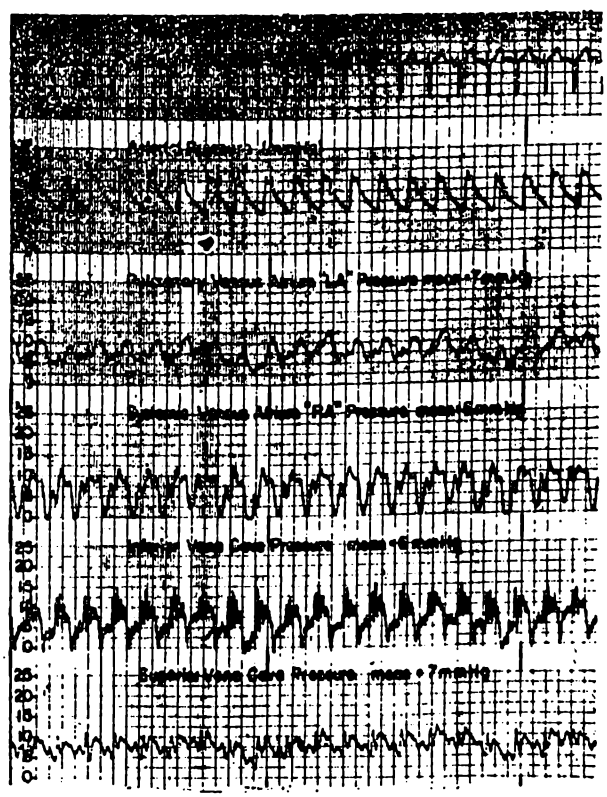

FIGURE 1: Pressure recording made four hours after the Mustard operation in a young child. Pressures are in mmHg. Paper speed was 25 mm/sec. (Figure 7 from [6], used by permission of The American Heart Association, Inc.)

ular the pressure waveform contour on the systemic and pulmonary venous sides of the interatrial baffle and in the superior and inferior vena cava. Pressure excursion in the systemic venous atrium is three to five times that observed in the normal right atrium. The excursion is somewhat less in the inferior vena cava (the tracing is contaminated by line noise) and even less in the superior vena cava. Mean (time averaged) pressures on both sides of the baffle are equal, whereas left atrial mean pressure is normally higher than that in the right atrium [7].

A few months postoperatively, when the usual ingrowth and deposition of fibrous material on the baffle has made it quite rigid, pressure waveforms such as those in Figure 2 are observed. These also show wide pressure excursions in the systemic venous atrium, although presumably there is now little pressure coupling through the baffle. Notice in this patient that the pressure in the superior vena cava is about two thirds of systolic pressure in the pulmonary (left) ventricle.

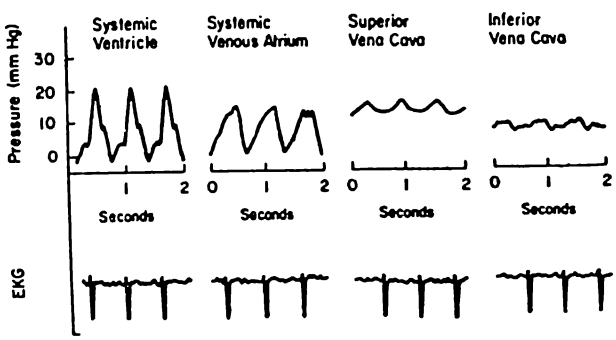

FIGURE 2: Nonsimultaneous pressure recordings made several months after the Mustard operation in a small child. The pressure monitoring catheter was pulled sequentially from chamber to chamber.

The infant's circulation after the Mustard operation was modeled to better understand the complexities resulting from the use of a flexible interatrial baffle. These included the effect of the altered atrial anatomy on venous return and on cardiac performance, the physiological effects of transatrial pressure coupling, the factors affecting final size of the atrial chambers when the baffle becomes stiff, and the factors which lead, in some cases, to apparent "obstruction" of venous return from the superior vena cava by the baffle operation [4]. This effort required the development of (a) a model of the circulation of a normal 10 kg infant (about one year old) since such a model had not been developed before, (b) a model of the effects of pressure coupling (interaction) between the new atrial chambers early post-operatively, and (c) a model of the atrial chambers after the baffle stiffens.

2. SIMULATION OF THE CIRCULATION OF A NORMAL INFANT

The techniques of modeling were based in large part on earlier work done at Wisconsin and elsewhere [8-16]. The lumped models of segments of arteries and veins were based on difference-differential equations derived from the Navier-Stokes equation for fluid flow [17], with collapsible segment models based on the work of Snyder [14-16].

The basic lumped pressure-flow model developed for a 10 kg infant has 25 segments, as shown in the block diagram (Figure 3), with three parallel paths in the systemic circulation. The corresponding circuit form of the model is shown in Figure 4; the equations for the pressures across and flows through each segment correspond to those for this electrical circuit, with parameter values in CGS units [17] given in Table 1.

The equations for a linear segment such as segment 1 are:

$$f_{22} - f_1 = C_1 \frac{d}{dt}[p_1 - R_{1w}(f_{22} - f_1)] \qquad (1)$$

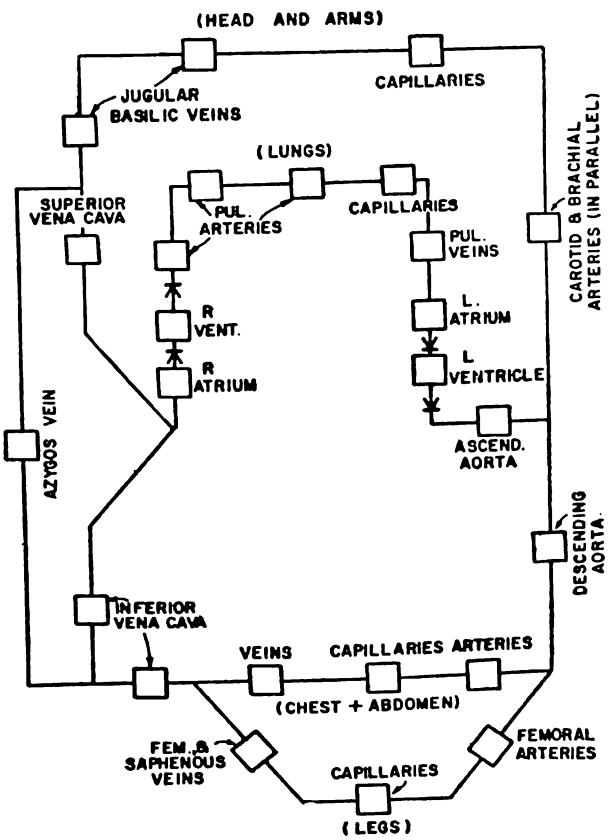

FIGURE 3: Block diagram of the model topology for the circulation of a normal 10 kg infant.

$$p_1 - p_2 = L_1 \frac{df_1}{dt} + R_1 f_1 \qquad (2)$$

where f_n and p_n are flows and pressures respectively. Resistances (R_n) and inertances (L_n) were found from assumed dimensions using formulas obtained from the Navier-Stokes equations.

$$R = \frac{8l\mu\ell}{8\pi a^4} \text{ (gm cm}^{-4}\text{ sec}^{-1}\text{)} \qquad (3)$$

where μ is viscosity (0.035 poise), ι is segment length (cm) and a is vessel radium (cm), and

$$L = \frac{9\rho\ell}{4\pi a^2} \text{ (gm cm}^{-4}\text{)} \qquad (4)$$

where ρ is blood density (1.06 gm cm^{-3}). Volume of any segment was given by

$$q = Q_u + q_s = Q_u + pC \qquad (5)$$

where Q_u is the unstressed volume, q_s is stressed volume and C is compliance. Q_u was assumed to be five times as large as $P_{ave}C$, where P_{ave} is average pressure in the segment. This relationship was used to find first approximations to compliances, C_n. Wall resistance R_{1w} [14] was assumed to be such that $R_{1w}C_1 = 0.02$ sec. In some segments, wall resistance was

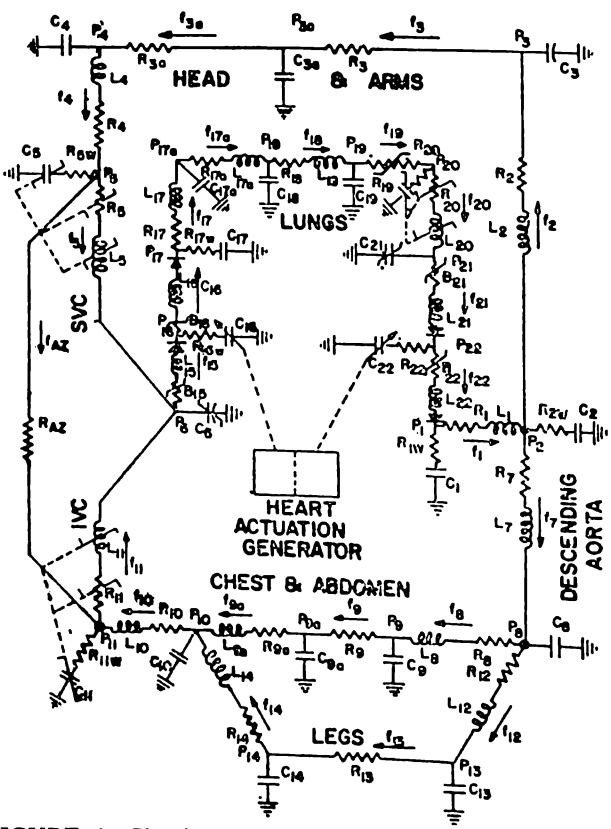

FIGURE 4: Circuit form for the circulatory model of Figure 3.

neglected, and in others, particularly capillary beds, L was omitted as well [12].

The pulmonary capillary resistance [18] was given by the hyperbolic relationship

$$P_{19}R_{19} = K \tag{6}$$

Segments 5 and 11 (superior and inferior vena cava) and segment 20 (pulmonary veins) were modeled to be collapsible, wtih compliances changing from the values in Table 1 to values 20 times greater as collapse began, and with L and R increasing as collapse progressed in a segment, are for the unstressed case, just before collapse begins. The compliances of the right atrium, C_6, and left atrium, C_{21}, are also nonlinear and were modeled with pressure-volume curves as defined in Figure 5.

The ventricles were modeled as time-varying nonlinear compliances with input and output valves (shown by rectifier symbols in Figure 4). The valve resistance is nonlinear with resistive pressure drop [19] given by

$$\Delta p = Bf^2 = \rho f^2/(2A^2) \tag{7}$$

where A is the area of the valve. The non-linear elastances (inverse compliances) of the ventricles were developed de novo for this modeling effort and are given as functions of volume by the curves of Figure 6, where $F_s\{q\}$ gives the pressure in full systole and $Fd\{q\}$ gives the pressure in diastole. The actual pressure generated depends on the time varying activation function $\alpha(t)$, shown in Figure 7, and ventricular volume where:

$$p = F_d\{q\} + \alpha[F_s\{q\} - F_d\{q\}] \tag{8}$$

The curves of Figure 6 were generated conveniently from algebraic expressions with parameters chosen to give good agreement with corresponding physiological curves. During ventricular diastole the pressure-volume relationship was assumed to have a Gompertz form:

$$q = Q_{max}\exp\ -In(Q_{max}/Q_u)\exp(\theta p) \tag{9}$$

or, after inversion,

$$p = F_d\{q\} = [In\ In(Q_{max}/Q_u) - In\ In(Q_{max}/q)]\ /\theta \tag{10}$$

For both ventricles the asymptotic volume $Q_{max} = 37$ ml and the unstressed volume $Q_u = 5$ ml (at $p = 0$). The shape factor $\theta = 0.145$ mmHg^{-1} for systemic ventricle and $\theta = 0.227$ mmHg^{-1} for the pulmonary ventricle. The curve describing the pressure-volume limits obtainable in the fully contracted ventricle was described by the exponential equation:

$$p = F_s\{q\} = P_{max}\ 1 - (1 - P_u/P_{max})\exp(-\beta q) \tag{11}$$

TABLE 1

$C_1 = 44$	$R_1 = 1.08$	$L_1 = 5.25$	$Q_{U_1} = 11.35$
$C_2 = 88$	$R_2 = 418$	$L_2 = 6.32$	$Q_{U_2} = 34.0$
$C_3 = 52.4$	$R_3 = 8\,220$	----	$Q_{U_3} = 19.0$
$C_{3a} = 1\,150$	$R_{3a} = 5\,200$	----	$Q_{U_{3a}} = 126$
$C_4 = 200$	$R_4 = 200$	$L_4 = 12$	$Q_{U_4} = 26.6$
$C_5 = 189$	$R_5 = 7.22$	$L_5 = 12.1$	$Q_{U_5} = 3.15$
C_6 (see Fig. 3)	$R_7 = 5.75$	$L_7 = 6.1$	----
$C_8 = 94$	$R_8 = 430$	$L_8 = 7.4$	$Q_{U_8} = 48.25$
$C_9 = 33.6$	$R_9 = 5\,350$	----	$Q_{U_9} = 12.3$
$C_{9a} = 1\,490$	$R_{9a} = 3\,570$	$L_{9a} = 47.4$	$Q_{U_{9a}} = 181$
$C_{10} = 308$	$R_{10} = 200$	$L_{10} = 6.2$	$Q_{U_{10}} = 6.15$
$C_{11} = 185$	$R_{11} = 1.88$	$L_{11} = 6.2$	$Q_{U_{11}} = 6.15$
----	$R_{12} = 645$	$L_{12} = 11.1$	----
$C_{13} = 29.6$	$R_{13} = 16\,400$	----	$Q_{U_{13}} = 10\,85$
$C_{14} = 506$	$R_{14} = 10\,800$	$L_{14} = 71.1$	$Q_{U_{14}} = 61.5$
----	$B_{15} = .054$	$L_{15} = 2.42$	----
C_{16} (see Fig. 4)	$B_{16} = .03$	$L_{16} = 1.8$	----
$C_{17} = 66$	$R_{17} = 6.32$	$L_{17} = 1.8$	$Q_{U_{17}} = 7.96$
$C_{17a} = 66$	$R_{17a} = 6.32$	$L_{17a} = 1.8$	$Q_{U_{17a}} = 7.96$
$C_{18} = 34.7$	$R_{18} = 90.6$	$L_{18} = 3.6$	$Q_{U_{18}} = 2.66$
$C_{19} = 223$	$R_{19} = 300$ (Ave.)	----	$Q_{U_{19}} = 12.25$
$C_{20} = 1\,310$	$R_{20} = 40.3$	$L_{20} = 8.3$	$Q_{U_{20}} = 39.16$
C_{21} (see Fig. 3)	$B_{21} = .054$	$L_{21} = 2.4$	----
C_{22} (see Fig. 4)	$B_{22} = .103$	$L_{22} = 1.5$	----
	$R_{AZ} = 26\,600$		

C's in cgs units $\times 10^6$, R's, B's, L's, and Q's in cgs units

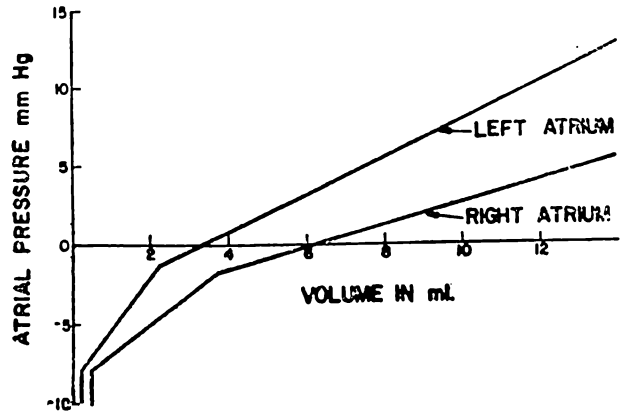

FIGURE 5: Left and right atrial pressure-volume curves used in the circulation model of the normal infant.

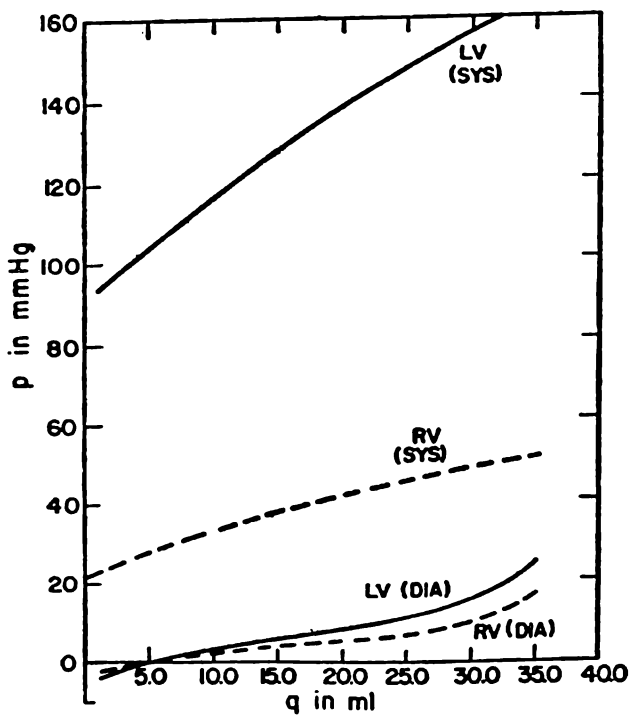

FIGURE 6: Pressure-volume curves for diastolic levels of heart excitation, LV(DIA) for left (or systemic) ventricle and RV(DIA) for right (or pulmonary) ventricle, and similarly for full systolic levels of excitation LV(SYS) and RV(SYS).

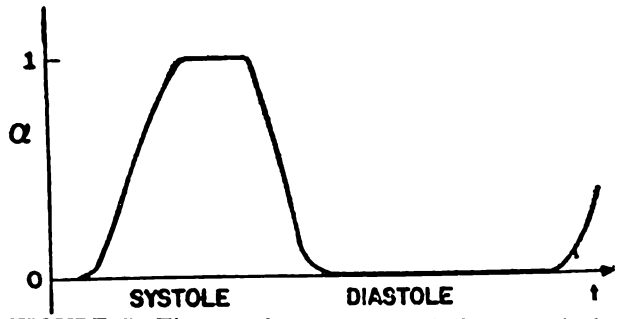

FIGURE 7: Time-varying curve used for ventricular excitation, $\alpha(t)$.

For the systemic ventricle P_{max}=237 mmHg, P_u=90 mmHg, and β=0.02 ml^{-1} while for the pulmonary ventricle P_{max}=63.8 mmHg, P_u=22.3 mmHg, and β=0.03 ml^{-1}.

Automatic control of heart-rate and strength of contraction can be added to this model by suitable feedback (as from carotid pressure [8], but only open-loop control on $\alpha(t)$ and P_{max} were used in the model studies to be described. Atrial pumping was also not included, and intrathoracic pressure was assumed to be zero (pressure fluctuations due to breathing were ignored).

The model was implmented on a hybrid computer system. After initial segment parameter values were obtained, they were improved by comparing waveforms in the model with those for a normal 10 kg infant, and by adjusting parameters to give better correspondence between human and model variables. The parameter values given in Table 1 and the final form of the curves shown in Figures 5, 6 and 7 were thus obtained.

The total blood volume of the system was computed by a digital computer program by first reading the pressure of each linear segment at the beginning of ventricular systole, calculating volume from this and the segments compliance, and then adding to each its unstressed volume. The sum of these volumes and those of nonlinear segments, given directly by function generators and integrators, yielded total blood volume. The difference between this volume and the reference volume (700 ml) was used to automatically control blood volume and thus to stabilize the system during simulation runs.

3. SIMULATION OF THE CIRCULATION OF INFANT AFTER THE MUSTARD OPERATION

A block diagram of the circulation of infants having TGA with intact ventricular septum is shown in Figure 8. This may be compared with the block diagram of the normal circulation in Figure 3. The inter-atrial communication created to provide mixing of blood between the two parallel circuits is indicated by the dashed line.

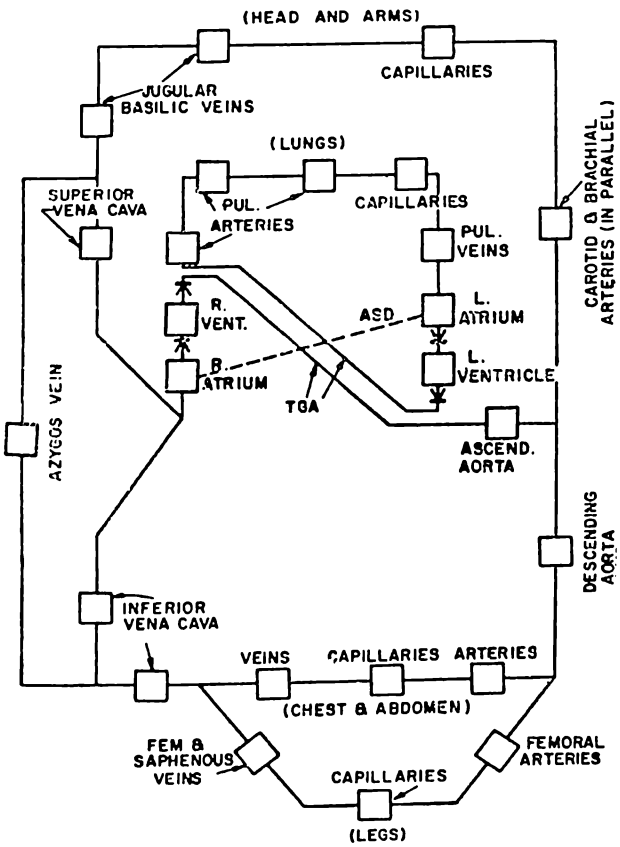

FIGURE 8: Block diagram of the model topology for the circulation of infants with TGA and intact ventricular septum in which the pulmonary and systemic riculations are isolated from one another. Life is possible if an atrial septal defect (ASD, dotted line) is present or is introduced.

When the Mustard operation is performed to interchange the venous returns, the remaining interatrial septum is removed, and a Y-shaped dacron or pericardial baffle is used to repartition the atrium as shown in Figure 9. The inferior vena cava (IVC) and superior vena cava (SVC) are connected to the two "legs" of the Y, and the common part of the baffle is placed over the mitral valve (this part of the stitching is not shown in the figure). The result, as shown in block form in Figure 10, is that the new systemic venous atrium (SVC), corresponding to the right atrium in the normal, is made of the main part of the Y and is partially inside the pulmonary venous atrium (PVA), the outer walls of which are those of the original atria. Notice that the ventricle on the right side is now the systemic ventricle (SV), and that on the left side is now the pulmonary ventricle (PV).

The new circuit geometry resulting after the Mustard operation, together with the collapsible characteristics of the new atria and of the intra-atrial conduits (the legs of the baffle), make for some problems in modeling. The problem of to-and-fro baffle motion because of pressure coupling between atria (i.e., interacting atrial chambers) was considered with the aid of Figure 11[a]. Here the PVA with internal pressure p_{21} is separated from the SVA with pressure p_6 by the baffle surface $S_{21,6}$. Outside pressures are p_a and p_b, and outside surfaces are $S_{21,a}$ and $S_{6,b}$. A dashed line represents an imaginary surface drawn to coincide with the baffle surface $S_{21,6}$ when it has zero transmural pressure ($p_6=p_{21}$). In the analysis that follows we need to define the volume q_{21} between the surface indicated by the dashed line and the wall $S_{21,a}$ as shown in Figure 11[b].

The inner (SVA) atrium has the volume

$$q_6 = q_6' + q_6'' \tag{12}$$

and the outer (PVA) atrium has the volume

$$q_{21} = q_{21}' - q_6' \tag{13}$$

If the various volumes are functions of the differential pressures, then

$$q_6' = F_6'\{p_6 - p_{21}\} \tag{14}$$

$$q_6'' = F_6''\{p_6 - p_b\} \tag{15}$$

$$q_{21}' = F_{21}''\{p_{21}' - p_a\} \tag{16}$$

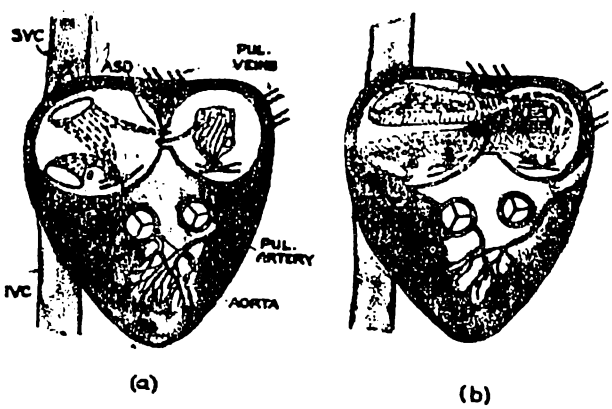

FIGURE 9: Sketch of the heart with TGA and after the Mustard operation. 9[a]: Abnormal heart circulation in an infant with TGA. Venous blood flowing through the vena cavae (dashed flow lines) goes into the right ventricle and on to the misplaced aorta, while oxygenated blood from the lungs (solid flow lines) goes into the left ventricle and back to the lungs. Life is possible because of a small amount of mixing through an atrial septal defect (ASD), as shown. 9[b]: Physiological correction using a dacron or pericardial baffle (Mustard operation) to conduct systemic venous blood to the mitral valve and left ventricle (pulmonary ventricle) and oxygenated blood to the tricusoid valve and right ventricle (systemic ventricle). Note that the atrial septum has been removed. (Redrawn from Breckenridge, I.M., et al.: Mustard's operation for transposition of the great arteries: Review of 200 cases. Lancet, May 27, 1140, 1972. Used by permission.)

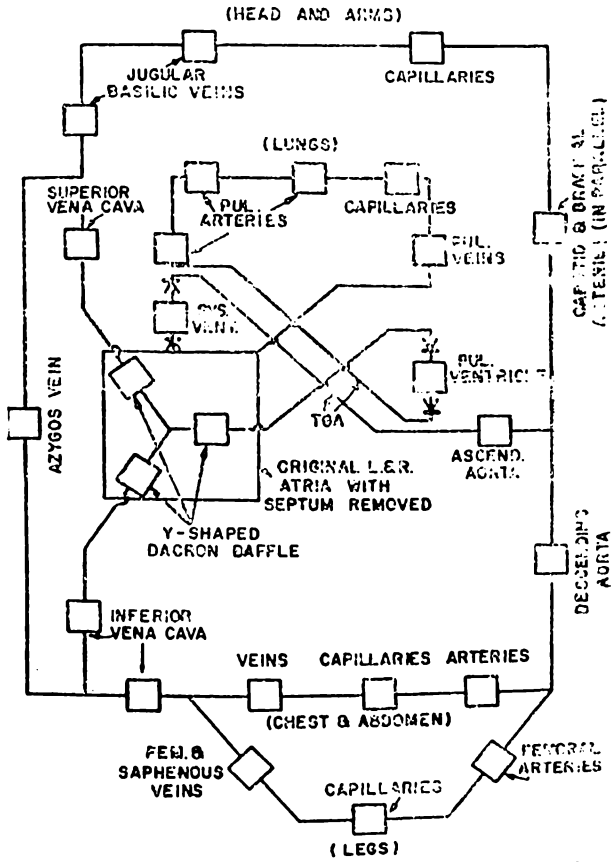

FIGURE 10: Block diagram of the model topology for the circulation after correction of TGA by interatrial transposition of venous return (Mustard operation).

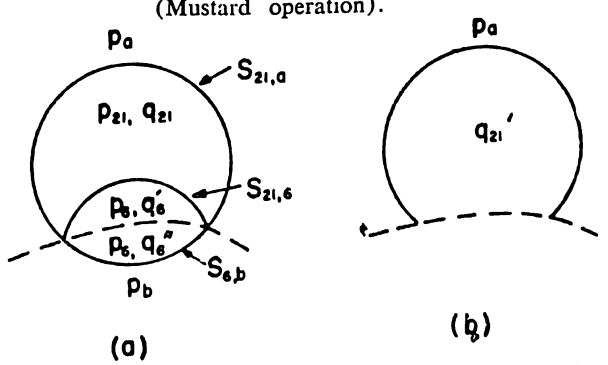

FIGURE 11: Idealized atrial cross-section after the Mustard operation. 11[a] shows the inner (SVA) atrium of volume $q_6=q_6'+q_6''$ and the outer (PVA) atrium of volume q_{21}. A theoretical surface (dashed line) is shown which corresponds to the baffle's position when $p_6=p_{21}$. 11[b]: Outer atrial cross-section with baffle surface $S_{21,6}$ absent, shown to define volume q_{21}'.

By combining equations (12) and (13) with (14), (15), and (16)

$$q_6 = F_6' \{p_6 - p_{21}\} + F_6'' \{p_6 - p_b\} \quad (17)$$

$$q_{21} = F_{21}'' \{p_{21} - p_a\} - F_6' \{p_6 - p_{21}\} \quad (18)$$

The curves used to define these pressure-volume relationships are shown in Figure 12. Notice that two of them have the usual shape of pressure-volume relationships for right and left atria (Figure 5) and taking a fractional part of this combined curve depending upon the relative estimated sizes of the SVA and PVA. The pressure-volume curve for the baffle is symmetrical about q = 0 since it was assumed to be capable of moving to-and-fro across the arbitrary surface (dashed line in Figure 11[a] coinciding with its zero transmural pressure. The baffle material is relatively non-distensible when stretched, and thus its pressure-volume curve was made rather flat over most of the positive and negative volume range. Finally, the slope of the pressure-volume curve of the "stiffened" baffle was assumed to be almost zero over the entire transmural pressure range. Its position on the volume axis was adjustable up and down, however, and simulation experiments were conducted to determine its probable position in the physiological setting.

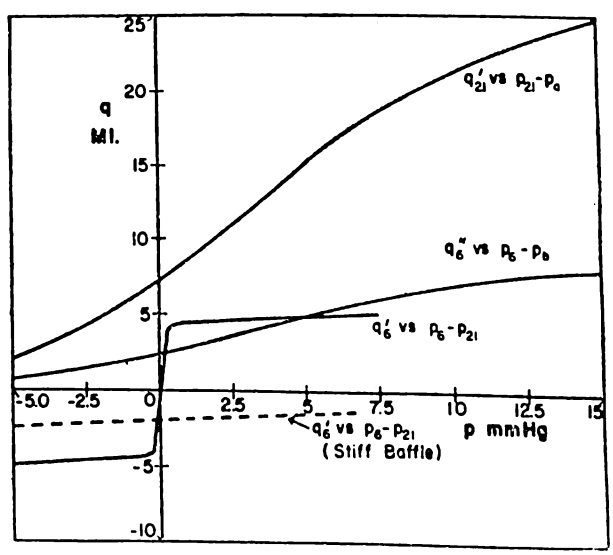

FIGURE 12: Pressure-volume curves for the three parts of Figure 11[a]. The curves for q_{21}' and q_6'' are identical except for a factor of 3, used because wall $S_{6,b}$ has smaller area than $S_{21,a}$. Also note that these curves are for natural atrial tissue, while the less distensible and more suddenly collapsible curves for q_6' is for dacron or pericardium, the size of which was obtained by averaging measurements of these materials used in several patients at surgery. The dotted line gives q_6' for the stiffened baffle state.

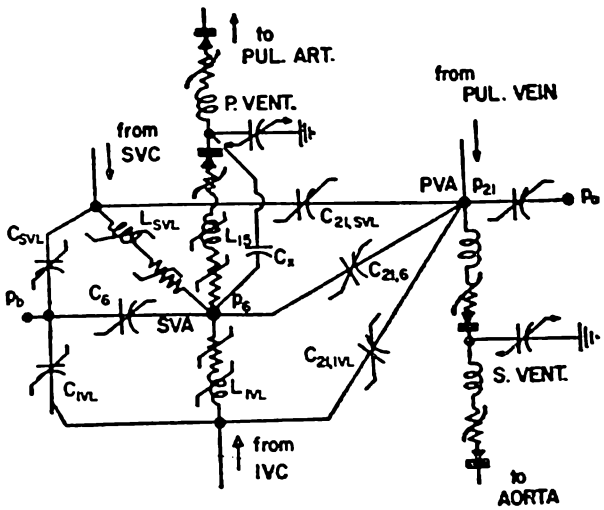

FIGURE 13: Partial circuit for an infant after the Mustard operation. When the new portions of this circuit are added to the circuit of Figure 4, the latter becomes a complete circuit model of the infant following the Mustard operation. C_x is a small capacity representing the effect of coupling of the ventricle to the atrium when the mitral valve is closed.

If linearized (17) and (18) become the equations for a π-circuit of compliances C_6, C_{21}, and $C_{21,6}$ (see Figure 13). This figure shows these compliances as nonlinear, and also shows similar ones connected to the systemic venous leg (SVL) and inferior venous leg (IVL) of the baffle, as well as showing the variable R's and L's of the added collapsible segments corresponding to the SVL and IVL. Numerical values of unstressed volumes (Q_u), resistances (R), and inertances (L), calculated for the SVA, these legs, and for the PVA at zero transmural pressure (in CGS units), are given in Table 2.

The analog computer set-up for the main part of the baffle required function generators for generating q'_6, q''_6, and q'_{21} according to the curves of Figure 21. These were used in a high-gain feedback circuit as shown in Figure 14 to generate p_6 and p_{21} given q_6, q_{21}, p_a and p_b as inputs. The simulation of each of the legs of the Y-shaped baffle required a similar set-up for interacting compliances, together with collapsible segment control of R and L.

4. COMPUTER SIMULATION STUDIES

Simulation studies of the normal infant, the infant immediately after the Mustard operation (soft baffle), and the infant some months postoperatively

(stiffened baffle) were made using the circulatory models described above. Figure 15 shows plots of pressure, volume and input flow (p_{21}, q_{21}, and f_{21}) for the pulmonary venous atrium together with the same variables for the systemic venous atrium together with the same variables for the systemic venous atrium (p_6, q_6, and f_{15}). The ventricular actuation function $\alpha(t)$ is included for purposes of timing events during the cardiac cycle. These variables are shown for the normal, the soft baffle, and the stiffened baffle states.

TABLE 2

	IVL	SVL	SVL	PVA
Q_u	2.83	1.32	3.80	11.4
R	2.18	10.00	0.4	—
L	5.28	11.30	1.8	1.2

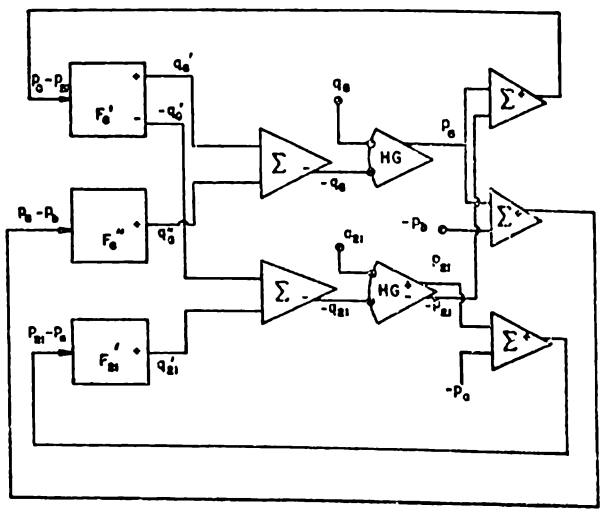

FIGURE 14: Analog computer set-up used to generate atrial pressures given volumes (from integration of flows) and external pressures p_a and p_b. A feedback scheme uses high-gain amplifiers (marked HG) to invert functions. This is a simplified diagram which does not show function generators, etc., for the legs of the baffle.

Notice in Figure 5 that there is little difference from state to state in pressure waveform contour in the PVA as contrasted to that in the SVA. The explanation for the contour of these waveforms in the simulation, which matches closely that actually observed (Figures 1 and 2), is as follows. The pressure in the atrium draining pulmonary venous blood is normally higher than that in the atrium draining systemic venous blood [7]. The primary determinants of this pressure differences between the properties of

the systemic and pulmonary ventricles. The systemic ventricle has a lower diastolic compliance (related to its wall thickness and geometry) and a higher afterload (which affects its end-systolic volume) near the pulmonary ventricle. Normally there is minimal pressure coupling across the atrial sentum, and thus the two pressures remain independent and nuequal. This is observed in the simulated waveforms of the normal infant (pressures p_{21} and p_6).

When the flexible baffle is introduced to repartition the atrium, pressure coupling between the atria occurs. This has several consequences. The generally higher PVA pressures causes a shift of the baffle past the arbitrary line in Figure 11[a] (i.e., q'_6 becomes negative). This results in an increased PVA volume (q_{21}) at the expense of volume in the SVA (q_6). Thus, unless there is impairment in the function of the pulmonary ventricle which results in an increase in its end diastolic pressure, the SVA will always tend to be relatively smaller than the PVA. Notice that during the simulation of ventricular systole, when the A-V valves are closed, SVA and PVA pressures tend to equalize.

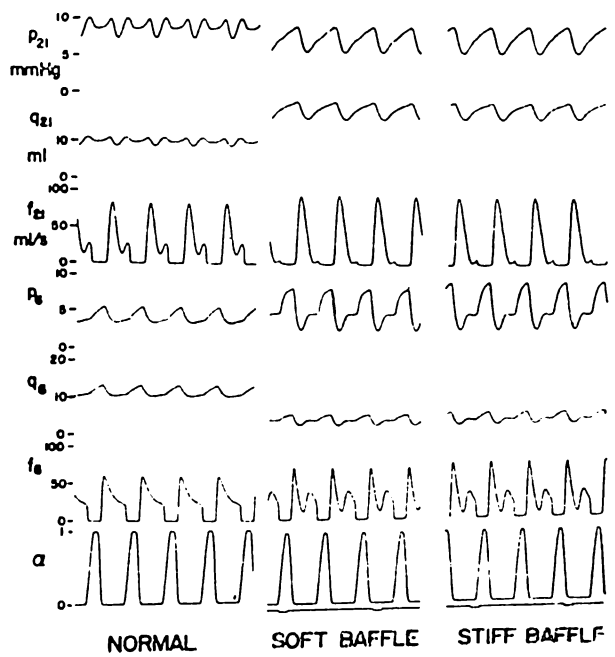

FIGURE 15: Computer generated plots of pressure, volume, and flow in the pulmonary venous atrium (p_{21}, q_{21}, and f_{21}) and in the systemic venous atrium (p_6, q_6, and f_6). The ventricular activation function $a(t)$ is included for timing of events according to the cardiac cycle. Paper speed is 25mm/sec. These side-by-side plots are for the normal infant and for both solft and stiff baffle states after the Mustard operation.

When the valves open during ventricular diastole, there is an initial high rate of flow into the ventricles (f_{21} and f_{15}) in the normal model which diminishes as the ventricle fills and respective atrial and ventricular pressures equalize. This flow pattern is essentially unchanged for f_{21} after the Mustard operation. However, the flow into the pulmonary ventricle (f_{15}) is greatly altered. As soon as the A-V valve opens, blood rapidly empties from the SVA into the pulmonary ventricle, precipitously dropping SVA pressure. This pressure drop is accentuated by the concommitant fall in PVA pressure due to flow into the systemic ventricle. Because the SVA is relatively small, the remainder of flow into the pulmonary ventricle must come from the large systemic veins, which lags to some extent. This results in a secondary flow across the mitral valve late in diastole during which time the SVA is acting as a relatively constant volume "tube" (see q_6). The net result is that pressure in the SVA is highly pulsatile. The pressure waveform is reminiscent of A-V valve incompetence; however, we believe that there is little or no incompetence of the mitral valve in the clinical setting, and the valve was modeled to have no backflow.

When the baffle stiffens, pressure coupling between the atria no longer significantly influences the atrial pressure waveforms. We have hypothesized, however, that the final position of the stiffened baffle, and thus the relative sizes of the systemic and pulmonary venous atria, is strongly influenced by its position when soft. In fact, simulation waveforms best matched those of Figure 2 when we positioned the stiff baffle on the volume axis (Figure 12) such that q_6 in the stiffened baffle state was similar to its average value in the soft baffle state. The simulation indicates that pressure pulsatility continues to be great in the SVA.

Figure 16 shows plots of pressure, volume, and flow in the superior (SVL) and inferior (IVL) caval limbs of the baffle. Notice that pulsatility is much less than in the SVA, which is replotted for reference. When the baffle stiffens, there is continued high pressure in these limbs. Lesser pulsatility and a higher mean pressure gradient between the SVL and the SVA can be simulated by hypothesizing a greater degree of collapse and constriction, and thus higher resistance to flow in the SVL. As the baffle stiffens in such a condition the flow velocity in the SVL becomes quite high and the pressure gradient quite large.

5. PHYSIOLOGICAL IMPLICATIONS FROM THE SIMULATION STUDIES

If we hypothesize that the mechanisms giving rise to the unusual pressure fluctuations in the simulation studies are those which produce similar waveforms in the clinical setting, then we may draw some physiological implications from the study. The simulation studies have emphasized the central importance of atrial pressure coupling across the soft baffle. It has indicated that if the normal relationship of atrial pressures as a reflection of the

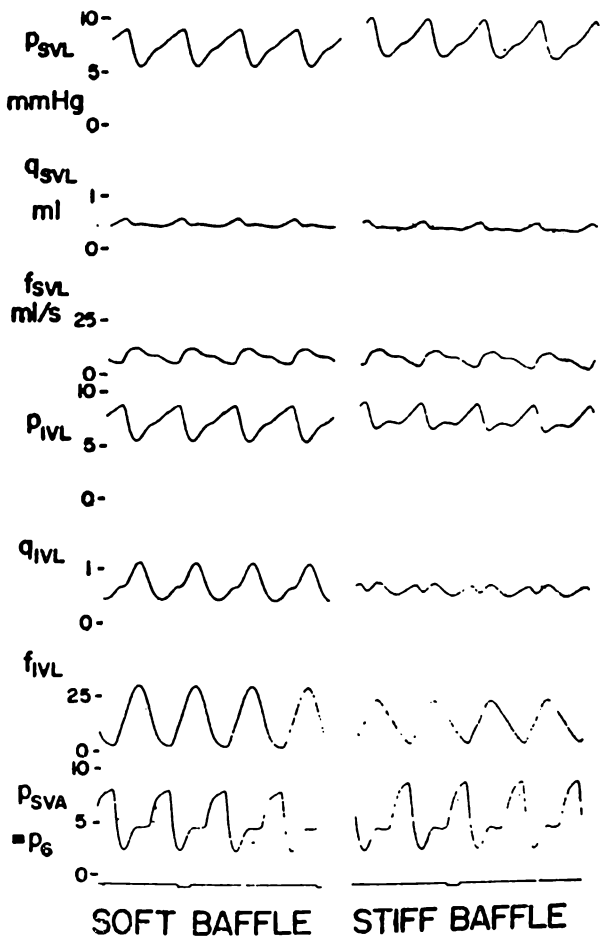

FIGURE 16: Computer generated plots of pressure, volume, and flow in the superior caval limb of the baffle (p_{SVL}, q_{SVL}, and f_{SVL}) and in the inferior caval limb (p_{IVL}, q_{IVL}, and f_{IVL}). The presence in the systemic venous atrium (p_{SVA}) is included for reference. Soft and stiff baffle states following the Mustard operation are shown side by side.

difference between the two ventricles holds, the baffle will always be shifted such that the SVA is smaller than the PVA, unless it can tethered in such a way as to prevent this coupling. This obligatory shifting is likely to make any early surgical revision of the baffle fruitless, since the relative smallness of the SVA and its limbs are not likely the result of poor operative techniques, but of the coupling phenomenon. This coupling would also appear to have direct influence on the final position the baffle takes as it stiffens.

The consequence of this is that high systemic venous pressure are maintained due to the permanently small size of the intra-atrial conduits and their consequently elevated resistance to flow. Systemic venous hypertension must tend to increase total systemic venous volume such that the ratio of systemic to pulmonary blood volume increases. Whether this hypertension will have long-term effects is as yet unknown.

The marked pulsatility of SVA pressure makes it hazardous to estimate ventricular filling pressure from an atrial pressure (as is employed clinically). However, the plateau observed in the phasic recordings is Figure 15 and also seen in the clinical tracings (Figure 1) is probably closest to ventricular end diastolic pressure. Note, however, that the usual ability to clinically evaluate the relative function of the two ventricles by observing the levels of the two mean atrial pressures is also lost due to the pressure coupling.

The simulation studies have not indicated that the Mustard operation directly affects cardiac performance. So long as ventricular filling pressure is maintained, cardiac performance would appear to be limited only by those factors affecting performance of the systemic ventricle, albeit with systemic and pulmonary blood volumes redistributed according to the pressure coupling. Since the baffle position is so strongly influenced by the factors affecting filling of the systemic ventricle, it is probably critical in this group of patients to allow this ventricle, it is probably critical in this group of patients to allow this ventricle to operate on the flattest part of its pressure-volume curve concommittant with adequate cardiac output. This implies that a good ejection fraction must be maintained and end-systolic volume minimized. This emphasizes the great importance of attention to afterload early postoperatively, for if systemic arterial pressure is abnormally high (which is often the case early after intracardiac surgery in infants 20), ejection fraction will be reduced and end-systolic volume will be increased. (A maneuver which can be done with the model, but not easily in man, is to relatively weaken the pulmonary ventricle; when this is simulated, the baffle tends to move to the PVA side and the size of the SVA increases.)

6. CONCLUSIONS

(1) A model of the complete circulatory loop of a normal 10 kg infant has been developed which incorporates a novel approach to ventricular modeling and multiple non-linear collapsible venous sections.

(2) A model of pressure coupling (interaction) between chambers of a repartitioned atrium has been developed as a model of the Mustard operation. This model describes both the case when the interatrial baffle is soft and when it stiffens. It was incorporated into the infant

model to simulate the post-surgical repair of transposition of the great arteries (TGA).

(3) Hybrid computer simulation studies of these models were performed which showed that the models generated unusual pressure waveforms quite similar to those observed clinically.

(4) The simulation studies emphasized the important physiological consequences of atrial coupling and have suggested ways in which post-operative care of such infants may be improved.

ACKNOWLEDGEMENTS

We wish to thank Dr. G. V. S. Parr for his help in developing the initial model of the 10 kg infant, Dr. J. W. Kirklin and Dr. A. D. Pacifico for their clinical data, and Dr. L. M. Bargeron, Jr. for the late catheterization data (Figure 2).

REFERENCES

[1] Lambert, E.C., Canent, R.V., Hohn, A.R.: Congenital cardiac anomalies in the newborn. A review of conditions causing severe distress in the first month of life. Pediatrics 37: 343, 1966.

[2] Rashkind, W.J., Miller, W.W.: Creation of an atrial defect without thoracotomy. A palliative approach to complete transposition of the great arteries. J.A.M.A. 196: 991, 1966.

[3] Mustard, W.T., Keith, J.D., Trusler, G.A., Fowler, R., Kidd, L.: The surgical management of transposition of the great vessels. J. of Thorac. Cardiovasc. Surg. 48: 953, 1964.

[4] Stark, J., de Laval M.R., Waterston, D.J., Graham, G.R., Bonham-Carter, R.E.: Corrective surgery of the great arteries in the first year of life: Results in 63 infants. J. Thorac. Cardiovasc. Surg. 67: 673, 1974.

[5] Anagnostopoulos, C. E., Athamasuleas, A. B., Arcilla, R.: Toward a rational operation for transposition of the great arteries. Ann. Thorac. Surg. 16: 458, 1973.

[6] Parr, G. V. S., Blackstone, E. H., Kirklin, J. W., Pacifico, A. D., Laudisen, P.: Cardiac performance early after interatrial transposition of venous return in infants and small children. Circulation 49-50: 11-2, 1974.

[7] Berglund, E.: Ventricular function: VI. Balance of left and right ventricular output: Relation between left and right atrial pressures. Am. J. Physiol. 178: 381, 1954.

[8] Beneken, J. E. W., DeWit, B.: A physical approach to hemodynamic aspects of the human cardiovascular system. In Physical Bases of Circulatory Transport: Regulation and Exchange, edited by Reeve, F. B., Guyton, A. C. Philadelphia, W. B. Saunders Co., 1967, p. 1.

[9] Westerhof, N., Bosman, F., deVries, C. J., Noordergraaf, A.: Analog studies of the human systemic arterial tree. J. Biomech. 2: 121, 1969.

[10] Dick, D. E.: A Hybrid Computer Study of Major Transients in the Canine Cardiovascular System. Ph.D. dissertation, University of Wisconsin, Madison, 1968.

[11] Snyder, M. F., Rideout, V. C., Hillestad, R. J.: Computer modeling of the human systemic arterial tree. J. Biomech. 1: 341, 1968.

[12] Rideout, V. C., Katra, J. A.: Computer simulation study of the pulmonary circulation. Simulation 14: 239, 1969.

[13] Rideout, V. C.: Cardiovascular system simulation in biomedical engineering education. IEEE Trans. Biomed. Eng. BME-19: 101, 1972.

[14] Snyder, M. F., Rideout, V. C.: Computer simulation studies of the venous circulation. IEEE Trans. Biomed. Eng. BME-16: 325, 1969.

[15] Snyder, M. F., Rideout, V. C.: The study of human venous system dynamics using hybrid computer modeling. NASA Report CR-2084, 1972.

[16] Snyder, M. F.: Modeling of venous system dynamics using hybrid computation. Proc. 1970 Summer Computer Simulation Conference, Denver, 1970, p. 1.

[17] Rideout, V. C., Dick, D. E.: Difference-differential equations for fluid flow in distensible tubes. IEEE Trans. Biomed. Eng. BME-14: 171, 1967.

[18] Kuchar, N. R.: Fluid dynamics in flexible tubes; An application to the study of the pulmonary circulation. NASA Annual Report, Contract No. NASW-2138, 1971.

[19] Bellhouse, B., Bellhouse, J.: Fluidic mechanics of normal and stenosed aortic valves. Circ. Res. 15: 693, 1969.

[20] Appelbaum, A., Blackstone, E. H., Kouchoukos, N. T., Kirklin, J. W.; Afterload reduction and cardiac putput in infants early after intracardiac surgery. Circulation (in press).